Eur. Phys. J. Special Topics **222**, 2705–2712 (2013)

DOI: 10.1140/epjst/e2013-02050-7

THE EUROPEAN PHYSICAL JOURNAL SPECIAL TOPICS

Regular Article

Wavelet-analysis of gastric microcirculation in rats with ulcer bleedings

A.N. Pavlov[1,a], O.V. Semyachkina-Glushkovskaya[2], O.N. Pavlova[1], O.A. Bibikova[2], and J. Kurths[3,4]

[1] Physics Department, Saratov State University, Astrakhanskaya 83, 410012 Saratov, Russia
[2] Biology Department, Saratov State University, Astrakhanskaya 83, 410012 Saratov, Russia
[3] Physics Department, Humboldt University, Newtonstrasse 15, 12489 Berlin, Germany
[4] Potsdam Institute for Climate Impact Research, Telegrafenberg A31, 14473 Potsdam, Germany

Received 16 July 2013 / Received in final form 13 August 2013
Published online 28 October 2013

Abstract. Nitric oxide (NO) plays an important role in regulation of central and peripheral circulation in normal state and during hemorrhagic stress. Because the impaired gastric mucosal blood flow is the major cause of gastroduodenal lesions including ulcer bleeding (UB), we study in this work the NO-ergic mechanism responsible for regulation of this blood flow. Our study is performed in rats with a model of stress-induced UB using laser Doppler flowmetry (LDF) that characterizes the rate of blood flow by measuring a Doppler shift of the laser beam scattered by the moving red blood cells. Numerical analysis of LDF-data is based on the discrete wavelet-transform (DWT) using Daubechies wavelets aiming to quantify influences of NO on the gastric microcirculation. We show that the stress-induced UB is associated with an increased level of NO in the gastric tissue and a stronger vascular sensitivity to pharmacological modulation of NO-production by L-NAME. We demonstrate that wavelet-based analyses of NO-dependent regulation of gastric microcirculation can provide an effective endoscopic diagnostics of a risk of UB.

1 Introduction

Severe ulcer bleeding (UB) is associated with a loss of gastric vascular tone and vascular reactivity to contractile agents [1]. Recent studies have proposed a hypothesis that an increased concentration of nitric oxide (NO) during hemorrhagic stress including gastrointestinal bleedings is produced by an activation of the inducible NO-synthase [2,3]. High levels of NO cause the opening of vascular smooth muscle channels leading to the development of hypotension and the resistance to vasopressors [4,5]. The

[a] e-mail: pavlov.lesha@gmail.com

elevated concentration of NO is an important factor for the increase in cyclic guanosine monophosphate resulting in an activation of myosin light-chain phosphatase and increasing of protein G kinase phosphorylation that opens K_{ATP} and K_{Ca} channels. The activation of these types of channels allows K^+ to leave the cell causing hyperpolarization, reducing of cytoplasmatic Ca^{2+} concentrations and vasodilation [6,7]. Taking into consideration these facts, here we test our hypothesis that an increased activity of the NO-ergic system (i.e., the system that carries out the synthesis and secretion of NO) in a stomach may be one of the crucial mechanisms responsible for pathological changes in the gastric microcirculation related with UB.

Aiming to quantify influences of NO on the gastric microcirculation, we perform experimental research using laser Doppler flowmetry (LDF) and the multiresolution analysis [6,7] based on the discrete wavelet-transform (DWT) being one of the most powerful tools for data processing. Wavelets are used here as the main mathematical approach because the considered time-series have non-stationary nature and they are complicated. Moreover, unlike the classical spectral analysis wavelets are more suitable to study time-frequency structure of physiological processes from quite short time series. Although many physiological applications of wavelets deal with the continuous transform of experimental data (see, e.g. [9–11]), DWT has some advantages. In particular, it is significantly faster such that signal processing can be realized in an "on-line" regime. Applying the discrete transform is also more natural in the case of digitized data (time series) and is used in practice if it is required to quickly compute some characteristics. Note, that wavelets have become now a basic mathematical tool in many studies including diagnostic problems in physiology and medicine. They often provide new insides into a complex structure of physiological time series and even reveal early stages of pathological changes in regulatory mechanisms that cannot be found with standard techniques such as, e.g., spectral or correlation analysis [12,13]. In our previous works, the efficiency of wavelet-based techniques for characterizing pathological changes in kidney microcirculation was shown [14–16] and a role of NO in the development of hypertension was discussed [17]. Here we study a role of nitric oxide in regulation of gastric microcirculation in rats with ulcer bleedings using "a language" of DWT-coefficients. These coefficients characterize the variability of a signal associated with different time scales. Their standard deviations can quantify the strenght of regulation of microcirculatory blood flow associated with different regulatory mechanisms.

2 Experiments

Experiments were performed in mongrel male rats (250 to 300 g) in accordance with the Guide for the Care and Use of Laboratory Animals published by the US National Institutes of Health (NIH Publication No. 85-23, revised 1996). The rats were housed at 25 ± 2^{o} C, 55% humidity, and 12:12 h light – dark cycle. Food and water were given *ad libitum*.

Gastric mucosal microcirculatory blood flow was studied using the laser Doppler flowmetry (LACC-2011 laser diagnostic complex, Moscow, Russia). The light from a HeNe laser (wavelength 635 nm) was focused on the tissue by an optical fiber, and the back-scattered light was detected by a pair of fibers with a separation of 0.5 mm. For the LDF probe in anesthetized rats with ketamine (Sigma Chemical Co, Saint Louis, USA, 40 mg/kg, iv), the abdomen was opened through a midline incision and the stomach was gently exteriorized. The forestomach was opened along the greater curvature and the rat was placed on its left side. To eliminate motion artifacts, the stomach was stabilized by placing it on a Perspex stage. The tip of either probe was positioned at about 0.5–1 mm from, and perpendicular to, the surface of the gastric

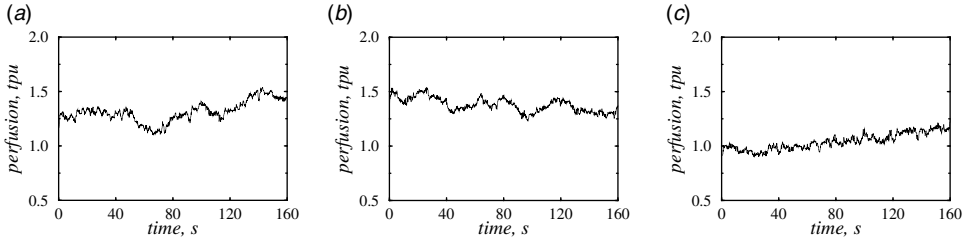

Fig. 1. Examples of LDF-data for a healthy rat (a) and for a rat with UB with (b) and without (c) NO-blockade.

mucosa. The duration of the recovering process was at least 1 hour after surgical preparation until mucosal blood flow was stabilized.

To induce the development of UB, rats underwent a combination of two types of stress: psychosocial chronic stress (overpopulation) and emotional stress (2 h immobilization). At the first stage of the experiments, rats were housed under chronic stress (overpopulation) during 4 months that was accompanied by a superficial mucosal damage in 83% of rats (61 of 73 rats used in our study). At the second stage, chronically stressed rats underwent another type of stress – 2 h immobilization (every day during 1 month). This additional daily stress induced the development of stress-related UB. Thus, the whole stressed period was 5 months.

LDF signals (perfusion, tpu) corresponding to control levels were measured for 10 min (30 min after the surgical procedure and stabilization of gastric mucosal blood flow), then submucosal injection of 0,1 ml N^G-nitro-L-arginine-methyl ester (L-NAME) being a non-specific blocker of NO-synthase (Sigma Chemical Co, Saint Louis, USA, 10 mg/kg) was applied and LDF signals were measured again for 10 min (immediately after L-NAME injection). The NO content in gastric tissue was measured by spectrophotometry (SF-2011, Moscow) using standard method described in [18]. We analysed LDF-signals of 73 healthy rats and 61 rats with stress-induced UB recorded with the sampling step 0.04 sec. For each rat, two states are considered: control dynamics (10 minutes) and dynamics after injection of L-NAME (10 minutes). Each time series contained about 15000 data points. An example of the recorded LDF-signal is given in Fig. 1.

3 Methods

A detailed analysis of LDF-data was performed using a multiresolution approach based on the DWT [8,19]. Unlike the continuous wavelet-transform, each scale considered within the DWT contains an independent non-overlapping set of information about the analyzed data in the form of wavelet coefficients. The latter are obtained by using a pyramidal (fast) decomposition of the signal [20]. Within the DWT, a signal is decomposed using a set of low-pass and high-pass filters given by vectors of $L = 2M$ coefficients (this ensures that we always deal with even numbers quantigying the length of wavelet-bases). These filters are constituted by the dilated and translated versions of the scaling function $\varphi(t)$ and the "mother" wavelet $\psi(t)$:

$$\varphi_{j,k} = 2^{j/2}\varphi(2^j t - k), \quad \psi_{j,k} = 2^{j/2}\psi(2^j t - k). \tag{1}$$

The relation between the functions on different scales for $\varphi(t)$ are given by the following expressions with L coefficients h_k:

$$\varphi(t) = \sqrt{2}\sum_{k=0}^{L-1} h_k \varphi(2t-k), \;\; \psi(t) = \sqrt{2}\sum_{k=0}^{L-1} g_k \varphi(2t-k), \tag{2}$$

where the filter coefficients h_k are computed numerically from the solution of the M-th power equation [8]. Higher M provide smoother wavelets that have better regularity properties and can be more appropriate for the analysis of experimental data with polynomial trends. However, high number of vanishing moments is not always the best choice and a comparison of different variants may be useful. In practice, the Daubechies wavelets D^L are typically considered [19]. The upper index L characterizes the number of coefficients, while the number of zero moments is equal to M. A higher rank makes it possible to retrieve information on features of higher orders contained in signals by ignoring polynomial behavior (trend) in the analyzed data. This is important in the study of nonstationary processes.

Any signal $x(t) \in L^2(R)$ on any level of resolution j_n can be decomposed as follows

$$x(t) = \sum_i s_{j_n,i}\varphi_{j_n,i}(t) + \sum_{j\geq j_n}\sum_i d_{j,i}\psi_{j,i}(t) \tag{3}$$

with the coefficients $s_{j,i}$ and $d_{j,i}$ containing information about the signal on different independent scales. Since the sequence of wavelet coefficients changes in time for nonstationary processes, their standard deviations for different scales are considered as quantitative characteristics of the analyzed data:

$$\sigma_j = \sqrt{\frac{1}{N}\sum_{i=0}^{N-1}[d_{j,i} - \langle d_{j,i}\rangle]^2}, \tag{4}$$

where N is the number of wavelet-coefficients of the considered level of resolution. The values σ_j quantify fluctuations in a signal associated with different time scales. They provide an informative characterization of the signal structure and can be useful for diagnostics purpose. Thus, in particular, a recent study based on a multiresolution approach [12] proposed a clinically significant measure of the chance of heart failure. Smaller σ_j are associated with more pronounced influences of physiological control mechanisms. Analysis of experimental data based on these characteristics enables us to separate effects of different regulatory systems.

The selection of the wavelet basis is one of the most important stages in data processing: an appropriately chosen basis makes it possible to reveal more details from the analyzed signal by analogy with an appropriate selection of the microscope lens. Aiming to optimize the selection procedure, we propose the following algorithm: Let us consider two different physiological states that should be separated in the course of data processing. The acquired processes associated with each state are analyzed within "floating" windows (1024 data points) to get information about the variability of σ_j that is not associated with the transitions between the states. Thus, we estimate mean values and standard deviations of the measure (4) for the two states $\overline{\sigma}_{j,1} \pm \delta_{j,1}$ and $\overline{\sigma}_{j,2} \pm \delta_{j,2}$. Further, by analogy with a characteristic used in [21] for patterns separation we compute the P-measure as follows

$$P_j = \frac{|\overline{\sigma}_{j,1} - \overline{\sigma}_{j,2}|}{(\delta_{j,1} + \delta_{j,2})/2}. \tag{5}$$

Larger P_j are associated with clearer distinctions between characteristics of the considered physiological states at the scale j. A comparison between (i) different wavelet

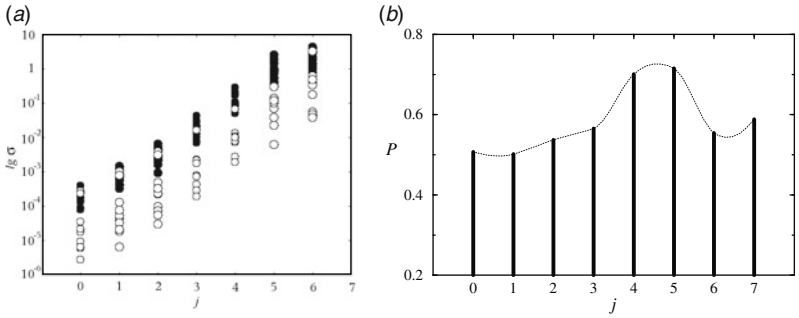

Fig. 2. Standard deviations σ_j of wavelet coefficients (Daubechies wavelets D^4) for a healthy rat (filled circles) and the same rat in the state of stress-induced ulcer bleedings (empty circles) (a) and the dependence P_j that reaches its maximal value for j=5 (b).

bases D^L of the Daubechies wavelets and, (ii) the scales described by the index j is performed to maximize the measure (5) and, therefore, to reveal a more essential discrimination between the experimental data.

4 Results

At the first stage of our study we tested the multiresolution approach providing estimation of the P-measure (5) for individual recordings. Figure 2 shows a typical example of how the given method discriminates standard deviations of wavelet-coefficients between the normal physiological state and the state of stress-induced ulcer bleedings. In the latter state, the values σ_j decrease testifying a stronger regulation of microcirculation by physiological control mechanisms. A reduction of σ_j is observed for each scale characterized by the index j. Let us consider the scales $j = 3$ and $j = 5$ associated with the low-frequency (around $f = 0.3\,\mathrm{Hz}$) and the high-frequency (around $f = 1.3\,\mathrm{Hz}$) cardiovascular dynamics [22,23]. Although the discrimination of σ_j occurs in both discussed frequency areas (Fig. 2a), the P-measure takes its maximal value in the case of the high-frequency dynamics corresponding to $j = 5$ (Fig. 2b). In Figure 2, the results are given for the simplest basis D^4 of the Daubechies wavelets. A consideration of higher ranks of the wavelet basis D^L may improve the discrimination of the analyzed physiological states; nevertheless, larger P-values will be obtained for the scales associated with the high-frequency dynamics. Let us note, that the control values of LDF do not demonstrate significant differences between individuals and between groups of healthy rats and animals with UB.

Further, we applied the multiresolution approach for the whole set of experimental data with the blockade of NO-synthesis. Figure 3a shows how mean values of σ_3 associated with the low-frequency dynamics (j=3) vary between different physiological states. Let us note that the values $\overline{\sigma}_3$ do not demonstrate clear distinctions between healthy and ill rats (Fig. 3a, triangles). Let us consider the ratio of mean standard deviations

$$r_j = \overline{\sigma}_{j,1}/\overline{\sigma}_{j,2} \tag{6}$$

where the numbers 1 and 2 denote different physiological states. Thus, for healthy and ill rats the ratio r_3 takes a value near 1.0 and, therefore, this measure is unable to uncover essential differences in the dynamics of the two groups. However, such distinctions can be revealed after the blockade of NO-synthesis that is resulted in a significant decrease of $\overline{\sigma}_3$. Following Fig. 3a, the measure r_3 for the states before and after the blockade takes a value near 2.0 for ill rats (filled circles) and near 1.7 for

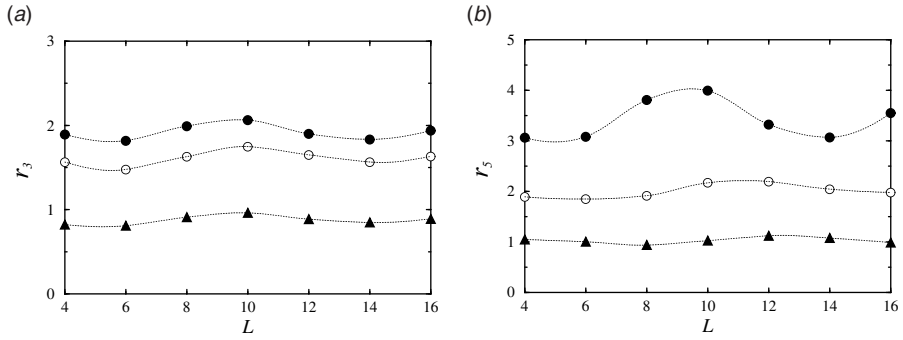

Fig. 3. The ratios r_3 (a) and r_5 (b) for healthy and ill rats before the blockade of NO-synthesis (filled triangles), for healthy rats before and after the blockade (empty circles), for ill rats before and after the blockade (filled circles). L is the number of coefficients of the considered wavelet-basis.

healthy rats (empty circles). A clearer group separation can be provided in the area of high-frequency dynamics ($j = 5$). Figure 3b illustrates how the distinctions between the groups of rats become more pronounced in this frequency region. Again, the used measure r_5 does not provide a separation between healthy and ill rats before the blockade of NO-synthesis (Fig. 3b, triangles). However, these two groups demonstrate different reactions caused by the injection of L-NAME. For healthy rats, the value $\overline{\sigma}_5$ before the blockade is about twice larger than after the blockade (Fig. 3b, empty circles).

The ratio of the corresponding mean standard deviations varies for different wavelets D^L, however, a choice of an appropriate wavelet is not critical. This situation essentially changes for the group of ill rats. The ratio of mean standard deviations takes values between 3.0 and 4.0 depending on the basis D^L. The reaction caused by the blockade is more expressed for the basis D^{10} as, e.g., for the basis D^4. Therefore, we can conclude that an appropriate choice of the basis can essentially improve diagnostics abilities of the multiresolution technique. We can also conclude that a study of high-frequency dynamics provides a way to clearly separate reactions of healthy and ill rats caused by the blockade of NO-synthesis.

Figure 3b illustrates also how the results depend on the selection of the basis. Thus, for the basis D^{10} the best discrimination between both groups of rats was obtained. For healthy rats, the measure (4) took the value $\sigma_5 = 0.08 \pm 0.03$(mean $\pm$ SD). The blockade of NO-synthesis provided a decrease of σ_5 up to the value 0.04 ± 0.01. For the group of rats with ulcer bleedings we did not found essential distinctions compared with healthy animals in the state before the blockade of NO-synthesis ($\sigma_5 = 0.09 \pm 0.02$). However, the blockade resulted in a decrease of the variability of the wavelet-coefficients up to the value $\sigma_5 = 0.02 \pm 0.01$, i.e. in about 4 times compared with 2 times for healthy animals. The latter testifies that the sensitivity of stomach vessels to the NO-dependent factors increases in rats with ulcer bleedings. We can also conclude that the used multiresolution approach demonstrates its high efficiency in the range of high-frequency dynamics. All differences between the groups are statistically significant.

Aiming to improve diagnostic abilities of the wavelet-based approach, we performed a comparison between different wavelet bases D^L for the whole sets of experimental data using the P-measure (5). Figure 4 illustrates an example of the dependence $P_j(L)$ for $j = 5$. By analogy with Fig. 3b, we can state that the maximal value of the P-measure is obtained for the basis D^{10}. Thus, the used measure provides indeed a way to automatically select an appropriate wavelet basis.

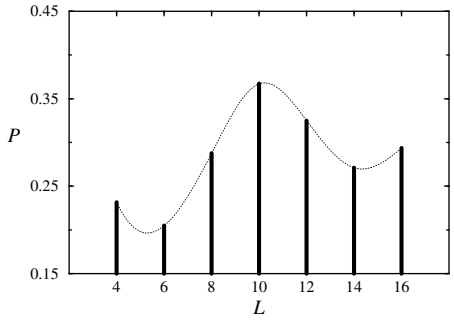

Fig. 4. The dependence of P_5 versus index L of the Daubechies wavelet bases D^L.

5 Conclusions

This study was undertaken to investigate the role of NO in regulation of gastric microcirculation in rats with UB using pharmacological modulation of NO production. Using submucosal injection of L-NAME, we studied the modulation of gastric perfusion after this injection in normal state (control group) and during UB (experimental group) in rats based on the DWT analysis of LDF signals. Our results show the clearest distinctions between the analyzed groups of rats in the high-frequency area. L-NAME provided a decrease of the variability of the wavelet-coefficients in about 2 times for healthy rats and in about 4 times for ill rats.

Note, that "a language" of DWT-coefficients is an effective way to study multiscale dynamics of physiological processes. Dispersion or standard deviation of these coefficients can serve as a measure of flexibility of the cardiovascular system. Here, we proposed an approach that enables us to select an optimal wavelet-basis providing the most distinct separation between different groups of animals.

The results based on a DWT analysis of the gastric microcirculation in the high-frequency area show that the gastric vascular sensitivity to NO blockade is higher in rats with ulcer bleeding than in healthy rats testifying the hyperactivity of the NO system under severe hemorrhages. L-NAME induces the vasoconstrictor effect and prolonged decrease in local gastric mucosal blood flow that is very important for endoscopic hemostasis. We assume that the endoscopic study of NO-dependent mechanisms of regulation of the gastric microcirculation during stress-related ulcer bleeding with the DWT-analysis can provide sensitive diagnostic markers for a risk of ulcer hemorrhages.

We would like to thank O.V. Ivanov for providing us with high-precision (64 digits) filters coefficients. This work was supported by the Russian Foundation for Basic Research (grants 11-02-00560-a, 12-02-31204) and by the RF Ministry of Education and Sciences within the Federal program "Scientific and scientific-pedagogic staff of innovative Russia for 2009-2013" (contracts 14.B37.21.0216, 14.B37.21.0853).

References

1. S.V. Kapralov, Y.G. Shapkin, V.V. Lychagov, V.V. Tuchin, Proc. SPIE **6535**, 653519 (2007)
2. C. Szabo, T. Billiar, Shock **12**, 1 (1999)

3. J. Collins, Y. Vodovotz, C. Hierholzer, R. Villavicencio, S. Liu, S. Alber, D. Gallo, D. Stolz, C. Watkins, A. Godfrey, W. Gooding, E. Kelly, A. Peitzman, T. Billiar, Shock **19**, 117 (2003)
4. D. Landry, J. Oliver, J. Clin. Invest. **89**, 2071 (1992)
5. J. Preiser, H. Zhang, F. Debelle, P. Fesler, S.A. Kafi, R. Naeije, J. Vincent, Shock **19**, 223 (2003)
6. J. Brayden, Clin. Exp. Pharmacol. Physiol. **29**, 312 (2002)
7. M. Nelson, J. Quayle, Am. J. Physiol. **268**, 799 (1995)
8. Y. Meyer (ed.), *Wavelets and Applications* (Springer-Verlag, 1992)
9. A. Aldroubi, M. Unser (eds.), *Wavelets in medicine and biology* (CRC Press, 1996)
10. P.S. Addison, *The Illustrated Wavelet Transform Handbook: Applications in Science, Engineering, medicine and Finance* (IOP Publishing, 2002)
11. O.V. Sosnovtseva, A.N. Pavlov, N.A. Brazhe, A.R. Brazhe, L.A. Erokhova, G.V. Maksimov, E. Mosekilde, Phys. Rev. Lett. **94**, 218103 (2005)
12. S. Thurner, M.C. Feurstein, M.C. Teich, Phys. Rev. Lett. **80**, 1544 (1998)
13. A.N. Pavlov, V.S. Anishchenko, Physics-Uspekhi **50**, 819 (2007)
14. D.J. Marsh, O.V. Sosnovtseva, A.N. Pavlov, K.-P. Yip, N.-H. Holstein-Rathlou, Am. J. Physiol. **288**, R1160 (2005)
15. A.N. Pavlov, V.A. Makarov, E. Mosekilde, O.V. Sosnovtseva, Briefings Bioinformatics **7**, 375 (2006)
16. O.V. Sosnovtseva, A.N. Pavlov, E. Mosekilde, K.-P. Yip, N.-H. Holstein-Rathlou, D.J. Marsh, Am. J. Physiol. **293**, F1545 (2007)
17. A.N. Pavlov, A.A. Anisimov, O.V. Semyachkina-Glushkovskaya, E.G. Matasova, J. Kurths, Physiol. Meas. **30**, 707 (2009)
18. J. Sun, X. Zhang, M. Broderick, H. Fein, Assay Sensors **3**, 276 (2003)
19. I. Daubechies, *Ten Lectures on Wavelets* (SIAM, 1992)
20. W.H. Press, B.P. Flannery, S.A. Teukolsky, W.T. Vetterling, *Numerical recipes in C: The Art of Scientific Computing* 2nd edn. (Cambridge, 1992)
21. V.A. Makarov, A.N. Pavlov, A.N. Tupitsyn, Proc. SPIE **6855**, 68550M (2008)
22. H.M. Stauss, Am. J. Physiol. **292**, R902 (2007)
23. H.M. Stauss, Clin. Exp. Pharmacol. Physiol. **34**, 362 (2007)